The Astrophysical Journal, 604:850–860, 2004 April 1

IMPROVED ATOMIC DATA FOR Ho II AND NEW HOLMIUM ABUNDANCES FOR THE SUN AND THREE METAL-POOR STARS

J. E. Lawler
Department of Physics, University of Wisconsin, Madison, WI 53706; jelawler@wisc.edu

C. Sneden
Department of Astronomy and McDonald Observatory, University of Texas, Austin, TX 78712; and
Carnegie Observatories, 813 Santa Barbara Street, Pasadena, CA 91101; chris@verdi.as.utexas.edu

AND

J. J. Cowan
Department of Physics and Astronomy, University of Oklahoma, Norman, OK 73019; cowan@nhn.ou.edu
Received 2003 September 19; accepted 2003 December 16

ABSTRACT

Improved energy levels and hyperfine structure constants for a selected set of Ho II levels were measured from spectra recorded using the 1 m Fourier transform spectrometer (FTS) at the US National Solar Observatory. Branching fractions for the strong blue-UV lines from these levels were also measured from the FTS data and combined with earlier radiative lifetimes from time-resolved laser-induced fluorescence measurements to determine accurate absolute transition probabilities for 22 lines of Ho II. These new laboratory measurements, along with a recently reported partition function for ionized Ho, were used to improve Ho abundance determinations in the Sun and three metal-poor Galactic halo giant stars. The derived solar photospheric holmium abundance, $\log_{10}\epsilon(\mathrm{Ho}) = +0.51 \pm 0.10$, is consistent with its meteoritic value, $\log_{10}\epsilon(\mathrm{Ho}) = +0.49 \pm 0.02$. In each of the metal-poor, neutron-capture–rich program stars, the holmium abundance relative to those of other rare earth elements agrees well with solar system rapid–neutron-capture abundance values.

Subject headings: atomic data — stars: abundances — Sun: abundances

1. INTRODUCTION

Holmium abundances in the Sun and other stars have been difficult to accurately determine. Some of the difficulty is due to the incomplete analysis of the spectrum. Most of the Ho II lines listed by Meggers, Corliss, & Scribner (1975) are unclassified (have unknown upper and lower levels). The available energy levels for Ho II (Martin, Zalubas, & Hagan 1978) are known to have errors of up to 0.5 cm^{-1} (Worm, Shi, & Poulsen 1990). Inaccurate energy levels and thus inaccurate wavelengths have made it difficult to identify Ho II lines with high confidence in solar and stellar spectra. Many lines of Ho II have wide hyperfine structure (HFS), which has slowed analysis of the spectra because of many line-blending problems. This HFS is sufficiently wide that it needs to be included in the analysis or synthesis of astrophysical spectra. Very few HFS constants for levels of Ho II are known (Worm et al. 1990; Sneden et al. 2003). Only a few modern, laser-calibrated transition probabilities have been published (Worm et al. 1990; Sneden et al. 2003).

J.-F. Wyart at the Laboratoire Aime Cotton has been working on the analysis of Ho II for some time (see the compilation and discussion by Martin et al. 1978). Radiative lifetimes for a few of the new Ho II levels that have been discovered by Wyart and for other known levels were reported by Den Hartog, Wiese, & Lawler (1999). The analysis of Ho II has progressed slowly in part because of the previously mentioned line-blending problems and in part because of configuration mixing, which has made it difficult to assign levels. Levels of the lowest even-parity configurations including the $4f^{11}6p$ and $4f^{10}\,(5d{+}6s)^2$ configurations are severely mixed. Although the lowest levels of the odd-parity $4f^{11}6s$ ground configuration are fairly pure, higher levels of this configuration are mixed with levels of the $4f^{11}5d$ configuration.

Bord & Cowley (2002, hereafter BC02) used the "Cowan Code" (Cowan 1981, 1995) to compute the approximate energies of many as yet unknown levels in Ho II and to improve the partition function of Ho II. Their work on the partition function brought the solar abundance of Ho into better agreement with the meteoric abundance of this element.

Recent studies of metal-poor Galactic halo stars have motivated much new laboratory work on spectra of the rare earth elements (Biémont & Quinet 2003). Abundance determinations of heavy neutron capture (*n*-capture) elements in very metal-poor stars have yielded new insights on the roles of the *r*(apid)- and *s*(low)-processes in the initial burst of Galactic nucleosynthesis (Gratton & Sneden 1994; McWilliam et al. 1995; Cowan et al. 1995; Sneden et al. 1996; Ryan, Norris, & Beers 1996). Improved laboratory data for La II (Lawler, Bonvallet, & Sneden 2001a), Eu II (Lawler et al. 2001c), Tb II (Lawler et al. 2001b; Lawler, Wyart, & Blaise 2001d), Nd II (Den Hartog et al. 2003), Ce II (Palmeri et al. 2000), Pr II (Ivarsson, Litzen, & Whalgren 2001), and other spectra have been recently published. Sneden et al. (2003) reported a small set of new laboratory measurements on Ho II as part of a study of CS 22892-052. Their work included improved energy levels and hyperfine constants for a few levels and branching fractions for four lines. The absolute scale for the Ho II transition probabilities reported and used by Sneden et al. was based on radiative lifetimes measured by Den Hartog et al. (1999) using time-resolved laser-induced fluorescence on Ho ions in a slow beam.

We have expanded the work on Ho II reported by Sneden et al. (2003) from four lines to 22 lines of Ho II, and we

have continued the analysis of laboratory emission spectra from hollow cathode lamps recorded using the 1 m Fourier transform spectrometer (FTS) at the National Solar Observatory (NSO). This paper contains an expanded set of accurate energy levels, HFS constants, and transition probability measurements for selected lines of Ho II, as well as more details on the Ho II laboratory results included in an appendix of Sneden et al.'s (2003) study of CS 22892-052. Some of the strongest lines of Ho II, from short-lived levels to the ground level or near-ground levels, were selected for this study. These lines were chosen as the most likely to yield clean abundance determinations. These new laboratory measurements were applied to determine the abundance of Ho in the Sun and three metal-poor Galactic halo giant stars.

2. FTS SPECTRA

Four spectra of Ho-Ar hollow cathode lamps recorded using the NSO 1 m FTS during a 1997 June observing run were used in this study. The 1 m FTS is a uniquely powerful instrument that provides (1) a limit of resolution as small as 0.01 cm^{-1}, (2) wavenumber accuracy to one part in 10^8, (3) broad spectral coverage from the UV to IR, and (4) the capability of recording a million-point spectrum in 10 minutes (Brault 1976). The FTS was operated with the UV beam splitter and "superblue" Si diode detectors during the 1997 June run. No additional filtering was used. All four spectra extend from 7929 to 34998 cm^{-1}, with a limit of resolution of 0.053 cm^{-1}. Small commercially manufactured sealed hollow cathode lamps were used during this study. The lamps were operated above the manufacturer's recommended currents, but forced-air cooling was used to prevent overheating. The Ho-Ar spectra included a spectrum with 10 co-adds at 10 mA lamp current, a spectrum with 10 co-adds at 20 mA current, a spectrum with 7 co-adds at 20 mA current, and a spectrum with 30 co-adds at 27 mA. Two spectra of Ho-Ne lamps were also recorded and used to check for possible blends between Ho lines of interest and Ar lines. The Ho-Ne spectra included a spectrum with 10 co-adds at 21 mA and a spectrum with 10 co-adds at 14 mA.

3. SELECTION OF LEVELS AND TRANSITIONS FOR DETAILED STUDY

The eight lowest levels of Ho II, including the ground level, belong to the $4f^{11}$ ($^4I^o$) $6s$ subconfiguration. The strong spin-orbit coupling of the f electrons separates this subconfiguration into four pairs of levels corresponding to the $4f^{11}$ ($^4I^o_{15/2}$) $6s$ pair, which is lowest, through the highest $4f^{11}$ ($^4I^o_{9/2}$) $6s$ pair. The lines most likely to be useful in abundance studies are the strongest lines connecting the low levels of the ground subconfiguration to levels of the $4f^{11}$ ($^4I^o$) $6p$ subconfiguration. The mixing between the $4f^{11}6p$ and $4f^{10}$ $(5d{+}6s)^2$ configurations complicates the task of identifying the $6p$ "resonance" levels with the strongest transitions to the ground and near-ground levels. In the absence of configuration mixing there would be six short-lived levels belonging to the $4f^{11}$ ($^4I^o_{15/2}$) $6p$ subconfiguration and six more belonging to the $4f^{11}$ ($^4I^o_{13/2}$) $6p$ subconfiguration. The first six of these short-lived levels should have strong lines to the $4f^{11}$ ($^4I^o_{15/2}$) $6s$ $J = 8$ ground level and $4f^{11}$ ($^4I^o_{15/2}$) $6s$ $J = 7$ metastable level near 637 cm^{-1}. The second six should decay primarily to the $4f^{11}$ ($^4I^o_{13/2}$) $6s$ $J = 7$ level near 5617 cm^{-1} and the $J = 6$ level near 5849 cm^{-1}. Some of these $6p$ "resonance" levels are known (Martin et al. 1978). Our approach has been to work from the level assignments given by Martin et al. (1978) and the radiative lifetime measurements of Den Hartog et al. (1999) to pick upper levels that have the strongest lines to the ground level and the three lowest metastable levels of the $4f^{11}$ ($^4I^o$) $6s$ subconfiguration. Although our immediate goal was to improve abundance determinations by focusing on the strongest lines connected to the ground or near-ground levels of Ho II, our laboratory results on Ho II may provide a better foundation for an expanded analysis of Ho II. The levels chosen for this study are in Table 1, with new results for the energy levels and HFS constants. The procedures used to generate these results are described in the next section.

TABLE 1

IMPROVED ENERGY LEVELS AND HFS CONSTANTS FOR ^{165}Ho II, $I = 7/2$

Configuration	Term	J	Energy (cm^{-1})	A (This Experiment)[a] (mK)	B (This Experiment)[a] (mK)	A[b] (mK)	B[b] (mK)
$4f^{11}$ ($^4I_{15/2}$) $6s_{1/2}$	(15/2, 1/2)^o	8	0.000	52.61	−53.9	+52.64 ± 0.07	−52.6 ± 3.3
$4f^{11}$ ($^4I_{15/2}$) $6s_{1/2}$	(15/2, 1/2)^o	7	637.754	0.86	−55.2	+0.83 ± 0.07	−56.4 ± 3.5
$4f^{11}$ ($^4I_{13/2}$) $6s_{1/2}$	(13/2, 1/2)^o	7	5617.456	+60.45 ± 0.07	−42.8 ± 3.5	+32.46 ± 0.23	−62 ± 16
$4f^{11}$ ($^4I_{13/2}$) $6s_{1/2}$	(13/2, 1/2)^o	6	5849.905	+2.83 ± 0.07	−46.5 ± 3.5	...	...
$4f^{11}$ ($^4I_{11/2}$) $6s_{1/2}$	(11/2, 1/2)^o	5	8850.560	+2.21 ± 0.07	−31.1 ± 3.5	...	...
$4f^{11}$ ($^4I_{11/2}$) $6s_{1/2}$	(11/2, 1/2)^o	6	9001.762	+67.78 ± 0.07	−46.6 ± 3.5	...	...
	...	7	24712.163	+42.16 ± 0.05	+1.7 ± 2.0	...	...
$4f^{11}$ ($^4I_{15/2}$) $6p_{1/2}$	(15/2, 1/2)	7	26234.363	+41.62 ± 0.05	+22.8 ± 2.0	...	...
$4f^{11}$ ($^4I_{15/2}$) $6p_{1/2}$	(15/2, 1/2)	8	26331.009	+31.27 ± 0.05	−30.7 ± 2.5	...	...
$4f^{11}$ ($^4I_{15/2}$) $6p_{3/2}$	(15/2, 3/2)	9	28926.815	+24.82 ± 0.07	+18.5 ± 3.5	...	...
	...	7	29325.350	+24.86 ± 0.05	−39.0 ± 2.0	...	...
$4f^{11}$ ($^4I_{15/2}$) $6p_{3/2}$	(15/2, 3/2)	8	29412.508	+26.60 ± 0.05	−62.8 ± 2.0	+26.52 ± 0.10	−60.7 ± 4.6
$4f^{11}$ ($^4I_{15/2}$) $6p_{3/2}$	(15/2, 3/2)	6	29588.888	+27.56 ± 0.07	+5.5 ± 4.0	...	...
$4f^{11}$ ($^4I_{15/2}$) $6p_{3/2}$	(15/2, 3/2)	7	29899.579	+24.09 ± 0.05	−27.7 ± 2.5	+24.02 ± 0.07	−26.8 ± 2.4
$4f^{11}$ ($^4I_{13/2}$) $6p_{1/2}$	(13/2, 1/2)	7	31556.613	+33.75 ± 0.07	−27.8 ± 3.5	...	...
$4f^{11}$ ($^4I_{13/2}$) $6p_{3/2}$	(13/2, 3/2)	6	35067.624	+33.29 ± 0.07	−50.8 ± 3.5	...	...

NOTE.—1.0 mK = 10^{-3} cm^{-1}.

[a] Parameters from Worm et al. 1990 for the two lowest levels were fixed during the initial least-squares fitting, then "relaxed" by one-half of an error bar for better internal consistency during the final least-squares fitting.

[b] Worm et al. 1990.

4. ENERGY LEVELS AND HYPERFINE CONSTANTS

Most of the broad HFS patterns of Ho II are resolved in our FTS spectra. Improved level energies and HFS constants were determined by least-squares fitting to the entire HFS patterns. Natural holmium has only one stable isotope, ^{165}Ho, with a nuclear spin $I = 7/2$. In this work we are using the Casimir formula as presented in the elementary text by Woodgate (1980). This formula is

$$\Delta E = \frac{AK}{2} + \frac{3BK(K+1) - 4I(I+1)J(J+1)}{8I(2I-1)J(2J-1)},$$

where ΔE is the shift in wavenumbers of an HFS sublevel (F, J) from the center of gravity of the fine-structure level (J),

$$K = F(F+1) - J(J+1) - I(I+1),$$

F is the total atomic angular momentum, J is the total electronic angular momentum, and I is the nuclear spin. The more advanced text by Cowan (1981) has an excellent discussion of HFS but uses a slightly different definition of the hyperfine B. Relative intensities of hyperfine components are expressed in terms of Wigner 6-j symbols by Cowan (1981). Some readers may find it more convenient to use the simple Russell-Saunders line strength formulae given in the classic text by Condon & Shortley (1935). The use of the Russell-Saunders formulae only requires substitution of F for J, J for L, and I for S. The diagonal ($\Delta F = \Delta J$) components are much stronger than the off-diagonal ($\Delta F \neq \Delta J$) components since transitions between levels with large J values were studied. Typically, the lines exhibit a classic HFS "flag" pattern with eight resolved or nearly resolved diagonal components, as shown in Figure 1. Proper relative intensities for the diagonal and off-diagonal components were included in fitting the patterns. Fitting parameters included the center of gravity of the line, the total intensity of the line, HFS A and B constants, and one line-profile parameter to approximate the convolution of the instrumental sinc function with a variable-temperature Doppler-broadened Gaussian line profile.

We experimented with using all four upper- and lower-level HFS A and B constants as fitting parameters but we were not satisfied with the stability of the fits. This has often been the case when we use FTS spectra to determine HFS constants

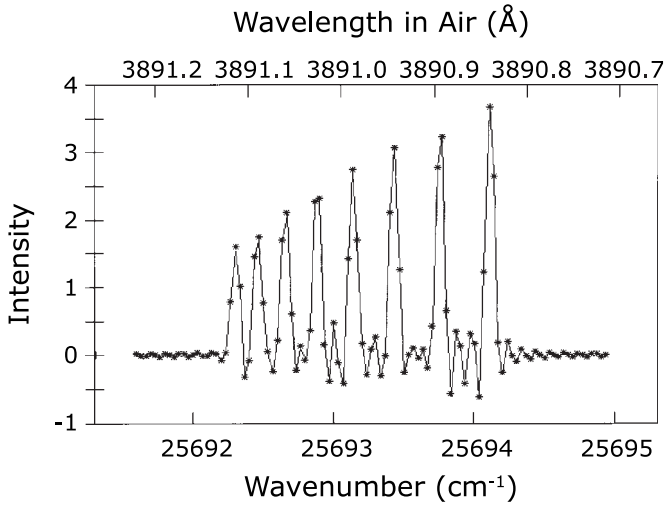

FIG. 1.—FTS data (*asterisks*) for the Ho II transition at 25693.25 cm^{-1} with a least-squares fit (*line*) superposed.

(e.g., Lawler et al. 2001d). The apodization of the interferogram produces some ringing on the instrumental profile. Although our fitting program includes a sinc instrumental profile for each HFS component, we still have some difficulty in accurately determining the position of the weak off-diagonal components. The weak off-diagonal components are overwhelmed by the ringing from the dominant diagonal components. In principal, this can be overcome by changing the apodization and recording higher resolution spectra, but signal-to-noise considerations and limited time in observing runs then become concerns. Accurate fitting of off-diagonal components is crucial to a simultaneous determination of the HFS constants of upper and lower levels. This is easy to understand by considering a $\Delta J = 0$ transition, since an increase of the upper-level HFS A is indistinguishable from a decrease of the lower level HFS A, if only diagonal components are observed. The problem is similar for $\Delta J \neq 0$ transitions. Our approach has been either to start from a $J = 0$ level and sequentially determine HFS constants of $J \neq 0$ levels, or to fix the HFS constants of one or more levels using values from the best published measurements. In the case of Ho II we fixed the HFS constants of the ground and lowest metastable level using the laser-induced fluorescence measurements of Worm et al. (1990). Worm et al. used a single-frequency laser on Ho ions in a well-collimated beam. Their reported values for the ground-level HFS A and B constants are based on their Doppler-free spectra of three different electronic transitions. Although their HFS A and B constants for the low metastable level near 637 cm^{-1} do not have the same degree of redundancy as the values for the ground level, we believe they are of comparable accuracy. We found quite consistent upper-level HFS A and B constants from fitting to pairs of lines in our FTS data that connected these two lower levels to a common upper level. In addition, an earlier but less accurate study of the HFS of the ground level (Sugar 1968) also supports the HFS constants reported by Worm et al. (1990) for the ground level. The choice of which HFS constants were to be fixed in our analysis was not trivial because the constants reported by Worm et al. for one level were found to be inaccurate.

The center of gravity of the transitions from the least-squares fits were used to refine the energy levels of Ho II. The primary accuracy issue in absolute wavenumber determinations from FTS data is the potential for a "rubber ruler" error from a misalignment between the reference laser and light beam from the lamp. This error scales as the cosine of the angular error, and it affects all wavenumber measurements by the same multiplicative factor. To test for this possible error, we used the same fitting program to study selected Ar II standard lines recommended by Learner & Thorne (1988). Their recommended 28 Ar II standard lines in the 19000–28000 cm^{-1} wavenumber range were chosen in part because of an insensitivity to pressure shifts. Leamer & Thorne suggested that their reported wavenumbers for these lines were accurate to ± 0.001 cm^{-1} or $\Delta\sigma/\sigma = \pm 4 \times 10^{-8}$. Whaling et al. (2002) have recently recommended a revision of Learner & Thorne's absolute wavenumbers with a multiplicative correction factor of $1 + 6.7 \times 10^{-8}$. Although this correction is slightly larger than Learner & Thorne's uncertainty, the independent test of their work gives us increased confidence in using the Ar II lines as wavenumber standards. Another issue of some concern in absolute wavenumber determinations is the phase correction of the interferogram (Learner et al. 1995). The phase correction was performed carefully. Any residual error in the phase correction could introduce a weak dispersion shaped part to the

instrumental profile, but it would affect the internal Ar II reference lines and Ho II lines in the same fashion. Clearly, internal standards for wavenumber and relative intensity measurements have important advantages. We used the exact same software to fit Ar II and Ho II lines. We have used the corrected Ar II wavenumbers to check for "rubber ruler" error in our spectra; we found and fixed such an error at the 10^{-7} level in one of the four spectra. Our recommended energy levels in Table 1 should be accurate to ± 0.003 cm^{-1}. This uncertainty corresponds to $\Delta E/E = \pm 10^{-7}$ for the radiating even-parity levels. The internal consistency of spectra recorded using the 1 m FTS is certainly better than the one part in 10^8 claimed in § 2, but the absolute scale requires some effort.

Our HFS A and B measurements in Table 1 have uncertainties based on the scatter in our least-squares results and based on the uncertainties of the A and B constants for the two lowest levels as reported by Worm et al. (1990). The agreement of our results for the even-parity levels at 29412.508 and 29899.579 cm^{-1} with the results of Worm et al. indicates that our uncertainty estimates are reasonable. We do not have an explanation for the discordance between our results and those of Worm et al. for the level at 5617.456 cm^{-1}, but we have considerable redundancy behind our reported HFS A and B constants for this level.

The set of levels in Table 1 were chosen because they are connected by some of the strongest lines terminating on the ground or near-ground levels of Ho II.

5. BRANCHING FRACTIONS AND TRANSITION PROBABILITIES

We used the now-standard technique based on overlapping sets of Ar I and Ar II branching ratios to establish a relative radiometric calibration for our Ho-Ar hollow cathode spectra. Sets of Ar I and Ar II lines have been established for this purpose in the range of 4300–35000 cm^{-1} by Whaling, Carle, & Pitt (1993), Hashiguchi & Hasikuni (1985), Danzmann & Kock (1982), and Adams & Whaling (1981). These provided an excellent means of calibrating our FTS spectra since the argon lines are measured in the exact experimental arrangement and at the exact same time as are the Ho II lines.

All possible transition wavenumbers between known energy levels of Ho II satisfying both the parity change and $\Delta J \leq 1$ selection rules were computed and used during analysis of FTS data. Energy levels from Martin et al. (1978), supplemented with some new levels from J.-F. Wyart (1999, private communication), were used to determine possible transition wavenumbers.[1] The selected levels typically have one or two strong blue-UV branches to low levels of the $4f^{11}$ ($^4I^o$) $6s$ subconfiguration.

Branching fractions from the FTS spectra were combined with the radiative lifetime measurements from Den Hartog et al. (1999) to determine absolute transition probabilities for 22 lines of Ho II in Table 2. Transition probabilities for the weakest lines, which were observed with poor signal-to-noise ratios, are not included in Table 2; however, these lines are included in the branching fraction normalization. Most of these weaker lines are near-IR branches to levels of the $4f^{11}5d$ configuration. Some of these IR lines were classified by Spector (1975, 1977) during work that led to his discovery of $4f^{11}5d$ levels. The last column of Table 2 is for comparison; it

[1] The levels from Martin et al. (1978) are available in electronic form from W. C. Martin, J. Sugar, & A. Musgrove (2003) at http://physics.nist.gov/cgi-bin/AtData/main_asd.

TABLE 2
ATOMIC TRANSITION PROBABILITIES FOR Ho II ARRANGED BY WAVENUMBER

Transition Wavenumber (cm^{-1})	λ in air (Å)	Upper Level (cm^{-1})	Upper J	Lower Level (cm^{-1})	Lower J	Transition Probability (10^6 s^{-1})	$\log_{10}(gf)$ This Experiment	$\log_{10}(gf)$ Other
30918.86.....	3233.34	31556.61	7	637.75	7	4.1 ± 0.8	−1.02	...
29899.58.....	3343.57	29899.58	7	0.00	8	14.1 ± 1.1	−0.45	−0.54[a]
29450.17.....	3394.59	35067.62	6	5617.46	7	16.1 ± 1.1	−0.44	...
29412.51.....	3398.94	29412.51	8	0.00	8	87 ± 5	0.41	0.27[b]
29325.35.....	3409.04	29325.35	7	0.00	8	3.05 ± 0.21	−1.10	...
29261.83.....	3416.44	29899.58	7	637.75	7	70 ± 4	0.26	0.23[a]
29217.72.....	3421.60	35067.62	6	5849.90	6	54 ± 3	0.09	...
28951.13.....	3453.11	29588.89	6	637.75	7	44.3 ± 2.2	0.01	...
28926.81.....	3456.01	28926.81	9	0.00	8	170 ± 9	0.76	...
28774.75.....	3474.27	29412.51	8	637.75	7	62 ± 3	0.28	0.18[b]
28687.60.....	3484.83	29325.35	7	637.75	7	70 ± 4	0.28	...
26331.01.....	3796.73	26331.01	8	0.00	8	39.7 ± 2.0	0.16	0.20[b]
26234.36.....	3810.71	26234.36	7	0.00	8	47.9 ± 2.4	0.19	...
26217.06.....	3813.23	35067.62	6	8850.56	5	38.3 ± 2.4	0.04	...
26065.86.....	3835.35	35067.62	6	9001.76	6	18.1 ± 1.2	−0.28	...
25939.16.....	3854.08	31556.61	7	5617.46	7	34.2 ± 1.8	0.06	...
25706.71.....	3888.93	31556.61	7	5849.90	6	63 ± 3	0.33	...
25693.25.....	3890.97	26331.01	8	637.75	7	75 ± 4	0.46	0.43[b]
25596.61.....	3905.66	26234.36	7	637.75	7	8.7 ± 0.4	−0.53	−0.66[a]
24712.16.....	4045.45	24712.16	7	0.00	8	24.2 ± 1.2	−0.05	−0.18[a]
24074.41.....	4152.62	24712.16	7	637.75	7	3.01 ± 0.16	−0.93	−0.89[a]
23738.98.....	4211.29	29588.89	6	5849.90	6	0.57 ± 0.05	−1.70	...

[a] VALD database as described in Kupka et al. 1999; value determined using the method of Magazzù & Cowley 1986.
[b] VALD database as described in Kupka et al. 1999; value originally from Gorshkov & Komarovskii 1979.

includes nine $\log_{10}(gf)$ values from the Vienna Atomic Line Database (VALD; Kupka et al. 1999).

The procedure used here for determining branching fraction uncertainties was described in detail by Wickliffe, Lawler, & Nave (2000). Branching fractions from a given upper level are defined to sum to unity; thus a dominant line from an upper level has small branching fraction uncertainty almost by definition. Branching fractions for weaker lines near the dominant line(s) tend to have uncertainties limited by their signal-to-noise ratios. Systematic uncertainties in the radiometric calibration are typically the most serious source of uncertainty for widely separated lines from a common upper level. In the case of the Ho II lines studied here, the relative strength of the dominant blue-UV branches were well determined, because these branches are strong and close together. The near-IR branches to the levels of the $4f^{11}5d$ configuration were more of a problem. Many of the near-IR branches to the $4f^{11}5d$ levels were near or slightly beyond the IR edge of our spectra, which is determined by the Si diode detectors. Even when near-IR lines were observed in the range from 9000 to 8000 cm^{-1}, it was sometimes difficult to determine accurate branching fractions because the sensitivity of the Si diode detectors varies so rapidly in this range. The near absence of branches between the strong blue-UV lines and the weak near-IR branches made it difficult to accurately "piece together" FTS spectra recorded using different detectors. We were able to measure all of the near-IR branches for the $J = 9$ level at 28926.815 cm^{-1}, and these branches were found to contribute 5% of the total decay from this level. Measurements of the near-IR branches from other levels in Table 1 were less complete and yielded contributions of less than 5% of the decay from those levels. We have included a flat 5% correction for IR branches from all levels in Table 1. This correction contributes a few percent uncertainty to some of the transition probabilities in Table 2; e.g., the strong blue-UV branches may be 97%–93% of the total decay from the upper level. Most of the uncertainty on the blue-UV transition probabilities in Table 2 is still from the $\pm 5\%$ uncertainty of the lifetimes.

6. THE ABUNDANCE OF HOLMIUM IN THE SOLAR PHOTOSPHERE

Until recently, a large discrepancy existed between the best estimates of the holmium abundance in meteorites, $\log_{10}\epsilon(\mathrm{Ho}) = +0.51$, and in the solar photosphere, $\log_{10}\epsilon(\mathrm{Ho}) = +0.26$.[2] A new study by BC02 proposes increasing the photospheric value to essentially equal that of meteorites. A large part of the proposed photospheric abundance increase comes from suggested changes in Ho II partition functions to account for atomic levels of this species that are predicted to exist but have yet to be observed in the lab. The remaining adjustment is due to a reanalysis of just a single Ho II line at 3416.44 Å. BC02 cautioned, however, that their newly determined abundance, $\log_{10}\epsilon(\mathrm{Ho}) = +0.53$, "is uncertain by at least 0.1 dex." Here the photospheric holmium abundance will be reassessed with our new lab data.

As in previous papers of this series, the first step was identification of promising solar Ho II transitions. Unfortunately, our preliminary spectral reconnaissance found no clean, strong features that could be used in this task. All 22 transitions in Table 2 occur in crowded spectral regions blueward of 4220 Å, and half of these occur below 3500 Å. Four of the lines are extremely weak [$\log_{10}(gf) \leq -1$]. In short, every one of our Ho II photospheric lines is very blended, very weak, or both.

Therefore we began the feature selection procedure not with the Sun but with the very metal-poor, neutron-capture–rich giant star CS 22892-052 (Sneden et al. 2003 and references therein; Den Hartog et al. 2003). Rare earth ionized species transitions are strong in this star, and the detection of a few Ho II lines has been previously discussed by Sneden et al. (1996, their § 4.1 and Fig. 5).

As a general rule, rare earth lines that are severely blended and/or undetectably weak in CS 22892-052 cannot be used in the solar photospheric analysis. Thus by examining the CS 22892-052 spectrum we quickly eliminated nine of the 22 possible lines for abundance analyses in the Sun or metal-poor stars: $\lambda\lambda$3233.34, 3409.04, 3835.35, and 4211.29 because they were too weak and $\lambda\lambda$3394.59, 3813.23, 3854.08, 3888.93, and 3905.66 because they were too blended.

For each of the remaining 13 lines we then constructed atomic and molecular line lists for small-wavelength regions (4–6 Å), beginning with the Ho II transitions themselves. Individual lines representing the 21–22 hyperfine subcomponents of each Ho II transition were constructed, using the data of Tables 1 and 2. Since natural holmium exists only as ^{165}Ho, consideration of isotopic wavelength offsets was unnecessary. Surrounding atomic and molecular (CH, CN, and NH) lines were taken from the Kurucz (1997)[3] line database. We also added a few lines identified in the solar spectrum by Moore, Minnaert, & Houtgast (1966) but missing from the Kurucz lists.

With these line lists, we then computed synthetic solar spectra with the current version of the LTE line analysis code MOOG (Sneden 1973), employing the Holweger & Müller (1974) empirical photospheric model. A microturbulent velocity of 0.85 km s^{-1} was adopted. We used the Ho II partition functions of BC02 (their eq. [1] and Table II); since holmium exists almost entirely in the first ion in the Sun and stars considered here, only the Ho II partition function affects the derived abundances.

The computed solar spectra were compared to the Delbouille, Neven, & Roland (1973)[4] center-of-disk solar spectrum. These comparisons were used to adjust iteratively the transition probabilities of atomic features (and to make very small line wavelength adjustments) to achieve satisfactory matches to the solar spectra. No adjustments were made to the Ho II components. Molecular line strengths were altered only as a group, through variations in assumed abundances of the molecular constituents. Finally, for a few absorptions in the solar spectrum with no plausible atomic/molecular identifications, we entered artificial Fe I lines with (arbitrary) excitation potentials $\chi = 3.5$ and freely adjustable gf-values to match the observed absorptions.

In 10 of the 13 synthesized spectral regions, holmium contributions to total line absorption could not be detected, because of weakness of the Ho II lines, great strength of the contaminating lines, or both. Such lines obviously were useless in determining a photospheric holmium abundance and will not be discussed further here. BC02 also considered using four of these lines ($\lambda\lambda$3474.27, 3796.73, 4045.45,

[2] For elements A and B, absolute abundances for the Sun or a star are defined as $\log\epsilon(\mathrm{A}) = \log_{10}(N_\mathrm{A}/N_\mathrm{H}) + 12.0$, and relative abundances between a star and the Sun are defined as $\log[\mathrm{A/B}] = \log_{10}(N_\mathrm{A}/N_\mathrm{B})_* - \log_{10}(N_\mathrm{A}/N_\mathrm{B})_\odot$.

[3] Available at http://kurucz.harvard.edu.

[4] Available at http://mesola.obspm.fr/solar_spect.php.

TABLE 3A

HOLMIUM ABUNDANCES AND ABUNDANCE UNCERTAINTIES IN THE SUN AND THREE METAL-POOR GALACTIC HALO STARS FROM SELECTED LINES OF Ho II

λ	Excitation Potential		Sun		CS 22892		BD +17°3248		HD 115444	
(Å)	(eV)	$\log_{10}(gf)$	Abund.	Unc.	Abund.	Unc.	Abund.	Unc.	Abund.	Unc.
(1)	(2)	(3)	(4)	(5)	(6)	(7)	(8)	(9)	(10)	(11)
3344.57.....	0.000	−0.45	...	...	−0.87	0.11	...	...	...	...
3398.94.....	0.000	0.41	0.54	0.15	−0.94	0.05	−0.66	0.02	...	...
3416.44.....	0.079	0.26	0.50	0.10	−0.92	0.02	−0.76	0.02	−1.67	0.10
3421.60.....	0.725	0.09	...	...	−0.91	0.10	−0.70	0.10	...	...
3453.11.....	0.079	0.01	...	...	−0.91	0.05	−0.75	0.10	−1.57	0.10
3456.01.....	0.000	0.76	0.50	0.10	−0.95	0.02	−0.73	0.02	−1.62	0.02
3474.27.....	0.079	0.28	...	...	−0.91	0.05	−0.70	0.05	−1.58	0.10
3484.83.....	0.079	0.28	...	...	−0.93	0.02	−0.72	0.05	−1.60	0.05
3796.73.....	0.000	0.16	...	...	−0.91	0.02	−0.70	0.05	−1.62	0.10
3810.71.....	0.000	0.19	...	...	−0.91	0.02	−0.70	0.10	−1.65	0.10
3890.97.....	0.079	0.46	...	...	−0.95	0.05	−0.70	0.05	−1.56	0.10
4045.45.....	0.000	−0.05	...	...	−0.91	0.05	−0.57	0.05	−1.58	0.10
4152.62.....	0.079	−0.93	...	...	−0.91	0.10	...	...	...	...

and 4152.62), and § 3 of their paper gives an excellent discussion of causes for the ultimate rejection of these lines.

Ultimately, we were able to use only the $\lambda\lambda$3398.94, 3416.44, and 3456.01 lines for a photospheric holmium abundance analysis. The derived abundances are given in Tables 3A and 3B, along with error estimates that account only for the uncertainties in matching observed and synthetic absorptions. BC02 also employed the λ3416 line for their study, and they dissected this transition in detail. We concur with their examination of this line and derive an abundance, $\log_{10}\epsilon(\mathrm{Ho}) = +0.50$, that agrees with their value (+0.53) to within the uncertainties of both studies.

Here we discuss briefly the λ3456 feature in the solar spectrum. This line should be the strongest of our Ho II transitions, about a factor of 2 larger than any other one. In the top panel of Figure 2 we plot vertical lines to represent the relative strengths of the hyperfine substructure components of this line. The total wavelength spread of this Ho II feature is 0.25 Å (a typical value for all of our transitions). There are 21 components plotted in the top panel of this figure, but just the eight diagonal ($\Delta F = \Delta J$) ones are strong enough to be clearly visible here. The total transition probability, $gf = 5.75$ (Table 2), is distributed primarily among these eight dominant components in the classic HFS flag pattern.

In the middle panel of Figure 2 we show the observed solar spectrum and synthetic spectra computed for four different assumed holmium abundances. Discussion of the CS 22892-052 spectrum in the bottom panel of Figure 2 is deferred to § 7. Only 2 Å surrounding the Ho II feature is shown here, but the total synthesized spectrum covered 6 Å to help in continuum placement in this obviously crowded wavelength region. A few general comments can be made from inspection of the solar synthetic/observed spectrum match. First, most major spectral features are reasonably accounted for, but important gaps remain (e.g., at 3456.3 and 3456.8 Å). Second, the Ho II transition is substantially blended in the solar spectrum, especially by the Fe II λ3456.01 line. This alone limits the precision to which the holmium abundance can be estimated. Third, the very large HFS of the Ho II transition actually helps in its positive identification because substantial holmium absorption in the solar spectrum is detected over a 0.2 Å wavelength range.

TABLE 3B

SUMMARY

Parameter	Sun	CS 22892	BD +17°3248	HD 115444
Average abundance.....	0.51	−0.92	−0.70	−1.61
p/m	0.01	0.01	0.02	0.01
σ	0.02	0.02	0.05	0.04
Number of lines.....	3	13	11	9

In Table 3A, columns (4) and (5) give derived solar abundances and their uncertainties for the three Ho II transitions. The quoted uncertainties account only for internal errors that arise from the synthetic/observed matches: continuum placement, line profile fitting, and blending feature confusion. The above remarks about the λ3456 Ho II line could apply equally well to the $\lambda\lambda$3398 and 3416 transitions. We concur with BC02 that abundances cannot be estimated from any solar Ho II feature to better than $\pm$0.1. It may be simply fortuitous that all three lines appear to yield abundances in good agreement with each other.

External (systematic) errors in the photospheric holmium abundance probably are not as large as the internal errors. The derived abundance does not depend on the assumed microturbulent velocity, because the Ho II lines are all very weak (and split into many weaker hyperfine components) in the solar spectrum. The choice of model solar atmosphere is more relevant, and adoption of either the Kurucz (1997) or Grevesse & Sauval (1998) model yields a lower holmium abundance by 0.03 dex. This is in accord with the abundance shifts found in our previous studies of other rare earth elements (Den Hartog et al. 2003 and references therein). Finally, the holmium abundance is very sensitive to the Ho II partition function. The solar abundance computed with a partition function formula based on currently known Ho II energy levels is about 0.08 dex less than one computed with the formula recommended by BC02 (which includes predicted levels not yet detected in the lab). The existence of many undiscovered levels in the low configurations of ionized Ho is unambiguous from counting various angular momentum projections. The Cowan Code calculation performed by BC02 is very likely to have produced approximately correct energies for the many

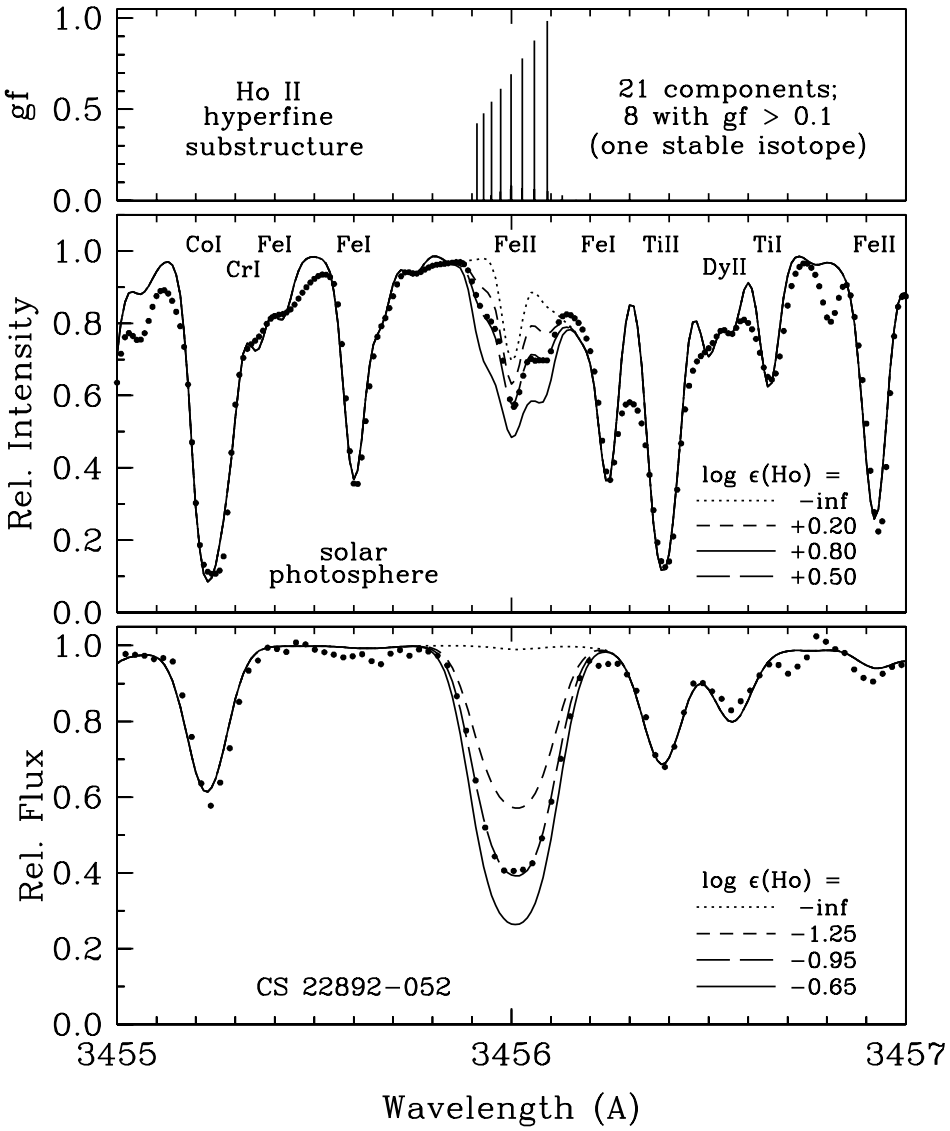

FIG. 2.—The λ3456.01 transition of Ho II. In the top panel we show vertical lines to represent the strengths and positions of the 21-component hyperfine structure of this transition. The eight diagonal ($\Delta F = \Delta J$) components dominate the HFS flag pattern. In the middle panel the observed solar spectrum (*filled circles*) is compared to four synthetic spectra with different assumed Ho abundances. The original Delbouille et al. (1973) center-of-disk solar spectrum has a wavelength step size of 0.002 Å in this spectral region, but for clarity we have only shown points in 0.01 Å steps. Most of the strongest absorbers in this small wavelength are labeled at the top of this panel. The assumed abundances in the calculations are given in the panel legend, with "−inf" denoting a synthesis with no contribution from Ho II. In the bottom panel the observed CS 22892-052 spectrum is also compared to four synthetic spectra.

undiscovered levels with excitation energies in the range from 10000 to 30000 cm^{-1}. Large numbers of undiscovered levels in this energy range do affect the partition function at solar photospheric temperatures but are less important at the lower temperatures characteristic of red giants. Given the current incomplete state of the analysis of Ho II, it is our opinion that BC02's partition function is the best available.

Adopting the straight mean abundance given in Table 3B, while ignoring the very small formal line-to-line scatter σ, we derive a solar photospheric abundance of $\log_{10}\epsilon(\mathrm{Ho}) = +0.51 \pm 0.10$. This value is in excellent agreement with the results of BC02 from just the λ3416 line. It also is in accord with (but does not constrain tightly) Lodders's (2003) recommended meteoritic solar system abundance, $\log_{10}\epsilon(\mathrm{Ho}) = +0.49 \pm 0.02$. Our study, taken together with BC02, gives no reason to suppose that conflict exists between meteoritic and photospheric values of holmium. This element joins other rare earth elements for which recent atomic lab results have led to reassessment of the photospheric abundances that in turn always have yielded better meteoritic/photospheric agreement.

7. HOLMIUM IN NEUTRON-CAPTURE–RICH METAL-POOR GIANTS

We have applied the new Ho II line data to three very metal-poor Galactic halo giant stars: CS 22892-052 ([Fe/H] = −3.1; Sneden et al. 2003), BD +17°3248 ([Fe/H] = −2.1; Cowan et al. 2002), and HD 115444 ([Fe/H] = −2.9; Westin et al. 2000). These stars all have large abundance excesses of *n*-capture elements relative to those of the Fe peak. The particular signature of the *n*-capture overabundances is clearly one of *r*-process dominance. That is, the abundance distribution among the heavy ($Z \geq 56$) *n*-capture elements is well matched by a scaled solar system distribution of just those parts of elements estimated to have been formed in rapid *n*-capture synthesis events (the *r*-process). The presence of

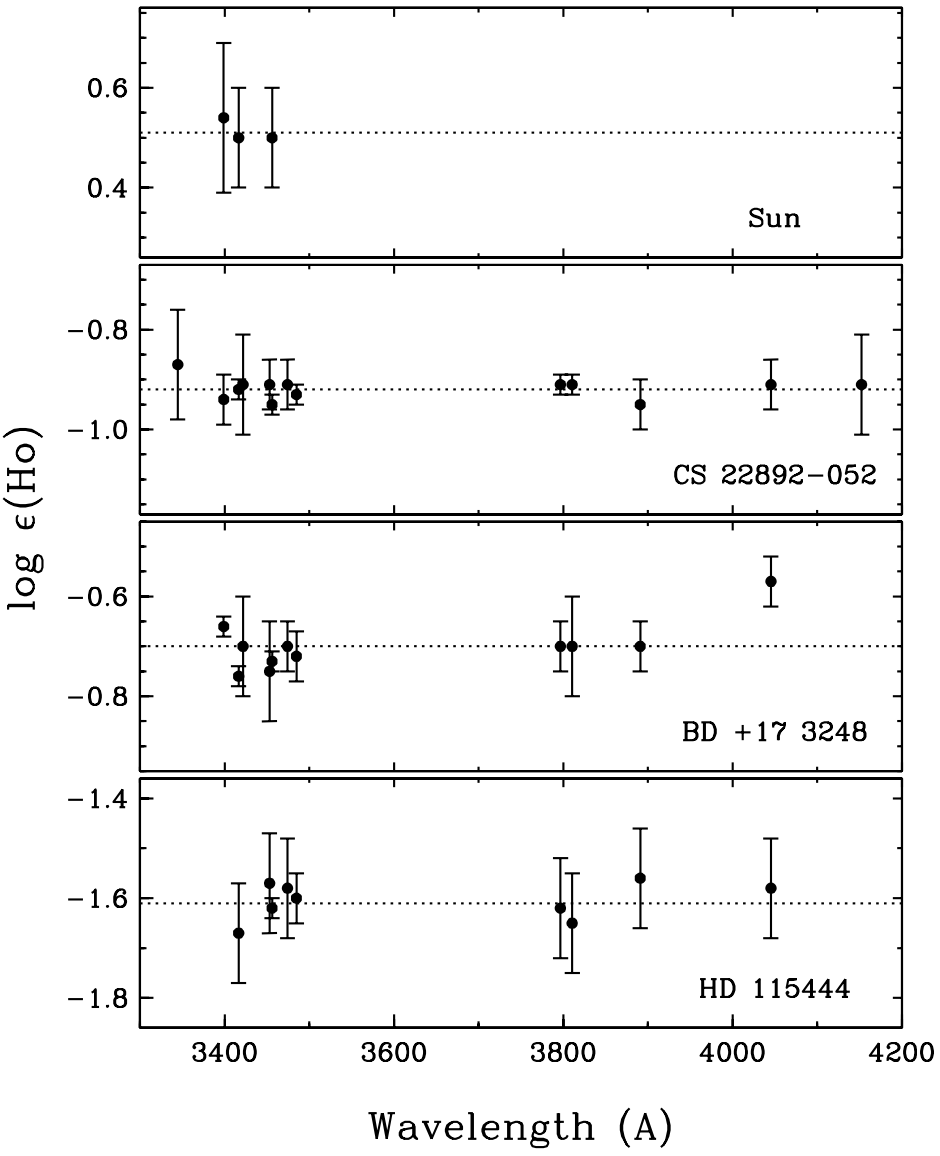

FIG. 3.—Holmium abundances determined from individual Ho II transitions plotted as a function of line wavelength, in the Sun and in three metal-poor, *n*-capture–rich stars. Derived mean abundances are indicated by horizontal dotted lines in each panel.

products of slow *n*-capture events (the *s*-process) cannot be detected in these stars.

We formed atomic and molecular line lists in the same manner as described for the solar analysis in § 6, but since the stars are very metal-poor and have factors of 5–40 relative *n*-capture abundance enhancements, many more Ho II features were clearly detectable and useful for detailed study. This is demonstrated in the bottom panel of Figure 2, showing the λ3456 transition in CS 22892-052. Comparing this spectrum with the solar spectrum in the middle panel of Figure 2 shows that the only significant absorptions are three Fe-peak lines (Co I λ3455.2, Ti II λ3456.4, and Fe II λ3456.8), the *n*-capture line Dy II λ3456.6, and the Ho II transition itself. The significant Fe II contaminant to the Ho II feature in the solar spectrum is barely detectable in the predicted CS 22892-052 spectrum. Clearly the Ho II feature dominates this spectral interval.

Application of the model atmospheres derived in the original studies of the three stars and line lists developed here yielded the abundances and internal uncertainties given in columns (6)–(11) of Table 3A. These abundances for each Ho II line in the stars and the Sun are displayed in Figure 3. The number of lines employed in CS 22892-052 is larger than, and the resulting line-to-line abundance scatter is smaller than, those of the other two stars. This is simply a result of the Ho II absorption contrast in this star: CS 22892-052 is more metal-poor than BD +17°3248 and HD 115444, and its *n*-capture abundances are more enhanced relative to the Fe-peak elements than they are in the other stars. But in all three stars the abundances derived from all Ho II transitions is in very good agreement (only the λ4045 line in BD +17°3248 appears somewhat discrepant). The holmium abundance is now well determined in these stars, and these line data may be applied with confidence to stellar spectra that do not have such strong Ho II features.

8. HOLMIUM AND IMPLICATIONS FOR THE *r*-PROCESS

We now revisit the Den Hartog et al. (2003) discussion of rare earth elemental abundances in the three *r*-process–rich metal-poor giant stars. The abundances for CS 22892-052 and

TABLE 4
ABUNDANCES OF *n*-CAPTURE ELEMENTS IN THREE *r*-PROCESS–RICH METAL-POOR STARS

	CS 22892-052			BD +17°3248			HD 115444		
ELEMENT	log ϵ	σ	Ref.	log ϵ	σ	Ref.	log ϵ	σ	Ref.
Ba	0.02	0.05	1	0.44	0.11	4	−0.68	0.09	5
La	−0.84	0.05	1	−0.42	0.05	4	−1.45	0.04	6
Ce	−0.50	0.07	1	−0.18	0.06	4	−1.10	0.12	5
Pr	−1.09	0.10	1	−0.71	0.05	4	−1.70	0.09	7
Nd	−0.37	0.06	2	−0.09	0.06	2	−1.02	0.08	2
Sm	−0.54	0.13	1	−0.42	0.14	4	−1.18	0.16	5
Eu	−0.95	0.03	1	−0.67	0.05	4	−1.63	0.02	8
Gd	−0.52	0.10	1	−0.26	0.09	4	−0.98	0.13	5
Tb	−1.13	0.05	1	−0.91	0.05	4	...	...	9
Dy	−0.23	0.08	1	−0.03	0.07	4	−1.01	0.10	5
Ho	−0.92	0.03	3	−0.70	0.06	3	−1.61	0.05	3
Er	−0.47	0.15	1	−0.20	0.06	4	−1.21	0.05	5

REFERENCES.—(1) Sneden et al. 2003; (2) Den Hartog et al. 2003; (3) this paper; (4) Cowan et al. 2002; (5) Westin et al. 2000; (6) this paper (six lines), atomic data from Lawler et al. 2001a; (7) this paper (four very weak lines), atomic data from Ivarsson et al. 2001; (8) this paper (eight lines), atomic data from Lawler et al. 2001c; (9) a few Tb II lines tentatively detected, but too weak and blended to yield a reliable Tb abundance.

BD +17°3248 are mostly adopted from the overall analyses of Sneden et al. (2003) and Cowan et al. (2002) cited in the preceding section. Updated Nd abundances have been taken from Den Hartog et al., and Ho abundances of course are newly determined here. However, the basic analysis of HD 115444 (Westin et al. 2000) predates all of the present series of papers on rare earth atomic transition probabilities. Therefore, for this star we have performed new abundance computations for La, Eu, and Pr (for which we have used the atomic data of Ivarsson et al. 2001).

In Table 4 we summarize the abundance of elements Ba ($Z = 56$) through Er ($Z = 68$), their abundance σ-values, the number of lines employed in the analyses of La, Pr, and Eu in HD 115444, and references to the abundance sources for each element in each star. In Figure 4 we display the differences of these three sets of rare earth abundances and those of the solar photosphere, with two independent assessments of solar system *r*-process–only abundances. The deconvolution of solar system total isotopic abundances into the various *r*- and *s*-process components has been obtained by first determining the *s*-process contributions on the basis of either the "classical" (empirical) approach (see, e.g., Käppeler, Beer, & Wisshak 1989) or the *s*-process nucleosynthesis models in low-mass asymptotic giant branch stars (Arlandini et al. 1999). Subtracting these *s*-process isotopic abundances from the solar totals determines the individual *r*-process contributions, which are then summed to obtain solar system elemental *r*- (and *s*-) process abundance distributions. The differences between stellar and solar system *r*-process abundances, called $\Delta[\log \epsilon(\mathrm{X})]$, have been arbitrarily normalized to force exact agreement at Eu, or $\Delta[\log \epsilon(\mathrm{Eu})] = 0.00$. Therefore, for a given star, perfect agreement between observed abundances and the solar *r*-process pattern will produce $\Delta[\log \epsilon(\mathrm{X})] = 0.00$ for all elements. Since the total solar photospheric rare earth abundances (*dotted line*) consist of both *r*- and *s*-process components, significant deviations in the positive direction should occur and are clearly seen in Figure 4. On the other hand, overall excellent agreement is seen between the abundances in CS 22892-052, BD +17°3248, and HD 115444 and the scaled solar system *r*-process distribution based first on the classical approach (Burris et al. 2000) shown in the top panel. The mean offset of the average of the three stars (by element and summed over all elements) and the solar *r*-process abundances is +0.04, with $\sigma = 0.06$; the difference is taken in the sense [(average of three stars) − (solar *r*-process)]. The solar system *r*-process abundances were taken from Burris et al. (2000) with one exception. The Nd value was revised to incorporate more recent measurements from Wisshak et al. (1998). We note that the stellar abundance data (incorporating new results from Den Hartog et al. 2003) for all three stars show very little difference from, and are in excellent agreement with, the revised prediction for solar *r*-process Nd. Moreover, the newly determined La and Pr abundances in HD 115444 are also in agreement with those in CS 22892-052 and BD +17°3248 and with the solar *r*-process. Further discussion and updated tabulations to the Burris et al. listings of the solar *r*-process predictions will appear separately in J. Simmerer et al. (2004, in preparation). The stellar elemental abundances in all three halo stars illustrated in Figure 4 (and listed in Table 4) are also consistent with the solar *r*-process abundances based on the *s*-process ("stellar") model calculations (*bottom panel*; Arlandini et al. 1999). A similar statistical comparison indicates that the mean offset of the average of the three stars with respect to the Arlandini et al. predictions is +0.04, with $\sigma = 0.05$. Those abundance predictions include one recent modification for the La value, which has been updated on the basis of new *n*-capture cross sections on ^{139}La (O'Brien et al. 2003).

This agreement between the abundances in the most metal-poor halo stars and the solar *r*-process curve has been noted previously in a number of earlier papers (see, e.g., recent reviews by Truran et al. 2002 and Sneden & Cowan 2003 and references therein). The results suggest first that at earliest times all of the elements were synthesized almost exclusively by the *r*-process. This includes so-called *s*-process elements such as Ba, which are overwhelmingly synthesized in the *s*-process in solar system material (see Truran et al. 2002 for further discussion). The agreement between the stellar abundances in the metal-poor stars (formed early in the history of the Galaxy) and the solar system abundances also suggests a robust *r*-process operating in a relatively consistent manner over many gigayears. As a result of the new laboratory

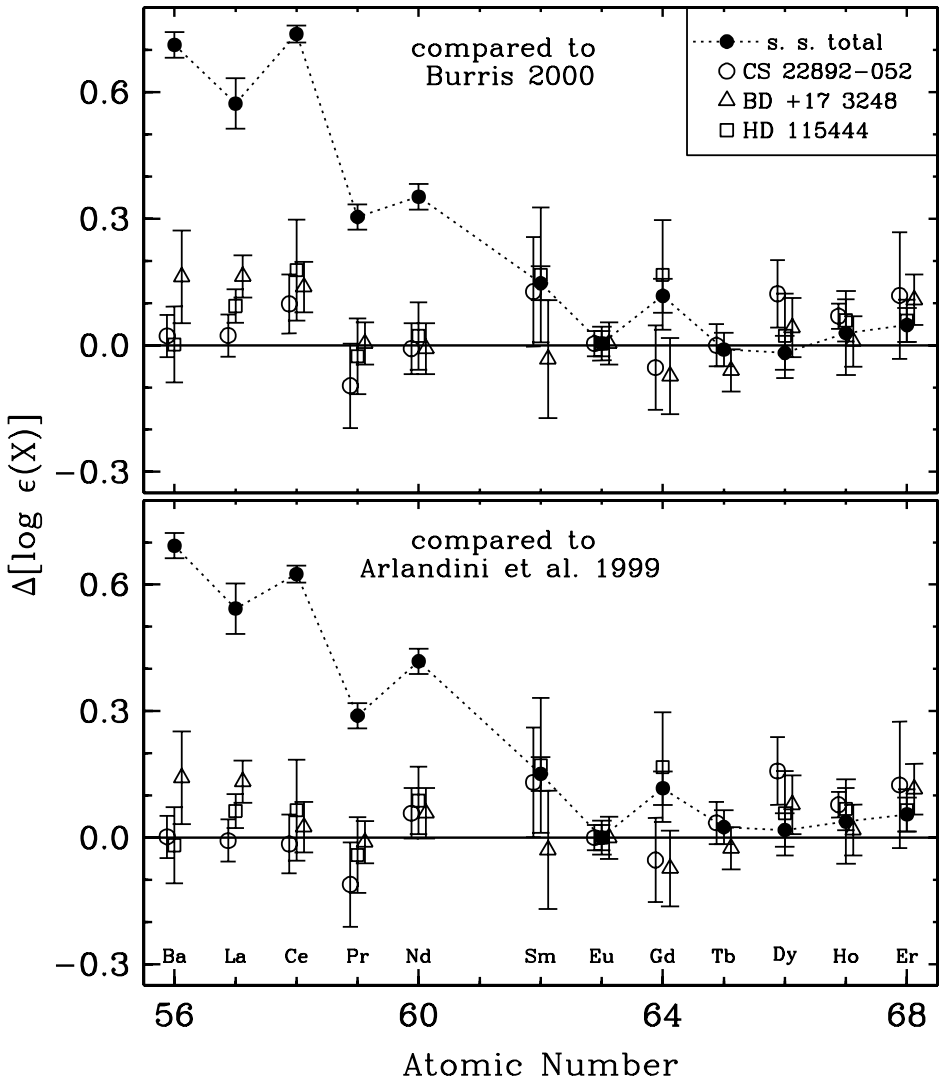

FIG. 4.—Differences between the *n*-capture abundances, from Ba to Er (scaled to Eu) in the metal-poor halo stars CS 22892-052, BD +17°3248, and HD 115444, with two predictions of the solar system elemental *r*-process abundances. Differences equal to zero, lying on the solid horizontal line, indicate perfect agreement with solar system *r*-process–only predictions. The total solar system (*s*- plus *r*-process) abundances are also shown for comparison.

measurements reported here, we have substantially improved the abundance determinations of the *r*-process element Ho (93% in solar material; Burris et al. 2000) in the three metal-poor halo stars and the Sun. In particular, we note the change in the Ho abundance for HD 115444. Earlier work had previously reported a value of $\log \epsilon = -1.81 \pm 0.11$, which appeared to be inconsistent (i.e., too low) with the other *n*-capture elemental abundance determinations (Westin et al. 2000). Our new measurement for this element in HD 115444, $\log \epsilon = -1.61 \pm 0.05$, now brings the abundance in this star in line with both the other metal-poor halo stars CS 22892-052 and BD +17°3248 and with the solar *r*-process distribution (see Fig. 4).

The availability of these increasingly precise atomic laboratory measurements are likely to have a number of important ramifications. First, improved abundance determinations for other elements in other stars may now be possible. We note, in particular, the cases of Sm and Gd illustrated in Figure 4, where there is evidence of significant abundance scatter from star to star. (New laboratory measurements and related stellar abundance determinations will be reported for Sm in J. E. Lawler et al. 2004, in preparation.) In addition, the improved atomic and stellar abundance data will be critical in helping to understand the formation history of the *n*-capture elements. For example, many of the details of the *r*-process, including the actual astrophysical site, are still unknown. Improvements in the stellar abundances in the old metal-poor halo stars, based on the new laboratory measurements, will provide a better understanding of this early Galactic nucleosynthesis history and help to identify the site for the *r*-process. Also, while in general there is good agreement between the two predictions for the solar *r*-process curve discussed above, there are some differences for some elements. The refined and more precise abundance determinations (with decreased scatter) will increasingly constrain, and will help to discriminate between, those theoretical predictions. Such refinements will ultimately lead to a better understanding of the details of both *r*-process and *s*-process nucleosynthesis.

This work is supported by the National Science Foundation under grants AST 02-05124 (J. E. L.), AST 99-87162 and AST 03-07495 (C. S.), and AST 99-86974 and AST 03-07279

(J. J. C.). J. E. Lawler is a guest observer at the National Solar Observatory and he is indebted to Mike Dulick and Detrick Branstron for help with the 1 m Fourier transform spectrometer. Parts of this research were accomplished while C. S. was a Visiting Scientist at Carnegie Observatories; their hospitality and financial support are appreciated. We thank Jason Collier for help in tabulating the *r*- and *s*-process contributions to the solar system abundances. We thank Roberto Gallino for helpful comments and for providing new results prior to publication. We thank the referee, D. J. Bord, for his conscientious efforts and suggestions, which improved our paper.

REFERENCES

Adams, D. L., & Whaling, W. 1981, J. Opt. Soc. Am., 71, 1036
Arlandini, C., Käppeler, F., Wisshak, K., Gallino, R., Lugaro, M., Busso, M., & Staniero, O. 1999, ApJ, 525, 886
Biémont, E., & Quinet, P. 2003, Phys. Scr., T105, 38
Bord, D. J., & Cowley, C. R. 2002, Sol. Phys., 211, 3
Brault, J. W. 1976, J. Opt. Soc. Am., 66, 1081
Burris, D. L., Pilachowski, C. A., Armandroff, T. A., Sneden, C., Cowan, J. J., & Roe, H. 2000, ApJ, 544, 302
Condon, E. U., & Shortley, G. H. 1935, The Theory of Atomic Spectra (Cambridge: Cambridge Univ. Press), 238
Cowan, J. J., Burris, D. L., Sneden, C., McWilliam, A., & Preston, G. W. 1995, ApJ, 439, L51
Cowan, J. J., et al. 2002, ApJ, 572, 861
Cowan, R. D. 1981, The Theory of Atomic Structure and Spectra (Berkeley: Univ. California Press), 508
———. 1995, Programs RCN/RCN2/RCG/RCE, Los Alamos National Laboratory
Danzmann, K., & Kock, M. 1982, J. Opt. Soc. Am., 72, 1556
Delbouille, L., Neven, L., & Roland, G. 1973, Photometric Atlas of the Solar Spectrum from λ3000 to λ10000 (Liège: Inst. Astrophys., Univ. Liège)
Den Hartog, E. A., Lawler, J. E., Sneden, C., & Cowan, J. J. 2003, ApJS, 148, 543
Den Hartog, E. A., Wiese, L. M., & Lawler, J. E. 1999, J. Opt. Soc. Am. B, 16, 2278
Gorshkov, V. N., & Komarovskii, V. A. 1979, Opt. Spectrosk., 47, 631 (English transl. in Opt. Spectrosc., 47, 350)
Gratton, R., & Sneden, C. 1994, A&A, 287, 927
Grevesse, N., & Sauval, A. J. 1998, Space Sci. Rev., 85, 161
Hashiguchi, S., & Hasikuni, M. 1985, J. Phys. Soc. Japan, 54, 1290
Holweger, H., & Müller, E. A. 1974, Sol. Phys., 39, 19
Ivarsson, S., Litzen, U., & Wahlgren, G. M. 2001, Phys. Scr., 64, 455
Käppeler, F., Beer, H., & Wisshak, K. 1989, Rep. Prog. Phys., 52, 945
Kupka, F., Piskunov, N. E., Ryabchikova, T. A., Stempels, H. C., & Weiss, W. W. 1999, A&AS, 138, 119
Kurucz, R. L. 1997, in IAU Symp. 189, Fundamental Stellar Properties: The Interaction between Observation and Theory, ed. T. R. Bedding, A. J. Booth, & J. Davis (Dordrecht: Kluwer), 217
Lawler, J. E., Bonvallet, G., & Sneden, C. 2001a, ApJ, 556, 452
Lawler, J. E., Wickliffe, M. E., Cowley, C. R., & Sneden, C. 2001b, ApJS, 137, 341
Lawler, J. E., Wickliffe, M. E., Den Hartog, E. A., & Sneden, C. 2001c, ApJ, 563, 1075
Lawler, J. E., Wyart, J.-F., & Blaise, J. 2001d, ApJS, 137, 351
Learner, R. C. M., & Thorne, A. P. 1988, J. Opt. Soc. Am. B, 10, 2045
Learner, R. C. M., Thorne, A. P., Wynne-Jones, I., Brault, J. W., & Abrams, M. C. 1995, J. Opt. Soc. Am. A, 12, 2165
Lodders, K. 2003, ApJ, 591, 1220
Magazzù, A., & Cowley, C. 1986, ApJ, 308, 254
Martin, W. C., Zalubas, R., & Hagan, L. 1978, Atomic Energy Levels—The Rare Earth Elements (NSRDS-NBS 60; Washington: GPO), 305
McWilliam, A., Preston, G. W., Sneden, C., & Searle, L. 1995, AJ, 109, 2757
Meggers, W. F., Corliss, C. H., & Scribner, B. F. 1975, Tables of Spectral Line Intensities (US NBS Monogr. 145; Washington: GPO), 105
Moore, C. E., Minnaert, M. G. J., & Houtgast, J. 1966, The Solar Spectrum 2934 Å to 8770 Å (US NBS Monogr. 62; Washington: GPO)
O'Brien, S., Dababneh, S., Heil, M., Käppeler, F., Plag, R., Reifarth, R., Gallino, R., & Pignatari, M. 2003, Phys. Rev. C, 68, 5801
Palmeri, P., Quinet, P., Wyart, J.-F., & Biémont, E. 2000, Phys. Scr., 61, 323
Ryan, S. G., Norris, J. E., & Beers, T. C. 1996, ApJ, 471, 254
Sneden, C. 1973, ApJ, 184, 839
Sneden, C., & Cowan, J. J. 2003, Science, 299, 70
Sneden, C., McWilliam, A., Preston, G. W., Cowan, J. J., Burris, D. L., & Armosky, B. J. 1996, ApJ, 467, 819
Sneden, C., et al. 2003, ApJ, 591, 936
Spector, N. 1975, Phys. Scr., 13, 181
———. 1977, ApJ, 211, 600
Sugar, J. 1968, J. Opt. Soc. Am., 58, 1519
Truran, J. W., Cowan, J. J., Pilachowski, C. A., & Sneden, C. 2002, PASP, 114, 1293
Westin, J., Sneden, C., Gustafsson, B., & Cowan, J. J. 2000, ApJ, 530, 783
Whaling, W., Anderson, W. H. C., Carle, M. T., Brault, J. W., & Zarem, H. A. 2002, J. Res. NIST, 107, 149
Whaling, W., Carle, M. T., & Pitt, M. L. 1993, J. Quant. Spectrosc. Radiat. Transfer, 50, 7
Wickliffe, M. E., Lawler, J. E., & Nave, G. 2000, J. Quant. Spectrosc. Radiat. Transfer, 66, 363
Wisshak, K., Voss, F., Käppeler, F., Kazakov, L., & Reffo, G. 1998, Phys. Rev. C, 57, 391
Woodgate, G. K. 1980, Elementary Atomic Structure (2nd ed.; Oxford: Clarendon), 184
Worm, T., Shi, P., & Poulsen, O. 1990, Phys. Scr., 42, 569